Aerodynamic benefits of boundary layer ingestion for distributed propulsion configuration

Jing Zhang
School of Automation Science and Electrical Engineering, Beihang University, Beijing, China
Wenwen Kang
Shanghai Aircraft Design and Research Institute, Shanghai, China, and
Lingyu Yang
School of Automation Science and Electrical Engineering, Beihang University, Beijing, China

Abstract

Purpose – Boundary layer ingestion (BLI) is one of the probable noteworthy features of distributed propulsion configuration (DPC). Because of BLI, strong coupling effects are generated between the aerodynamics and propulsion system of aircraft, leading to the specific lift and drag aerodynamic characteristics. This paper aims to propose a model-based comprehensive analysis method to investigate this unique aerodynamic.

Design/methodology/approach – To investigate this unique aerodynamics, a model-based comprehensive analysis method is proposed. This method uses a detailed mathematical model of the distributed propulsion system to provide the essential boundary conditions and guarantee the accuracy of calculation results. Then a synthetic three-dimensional computational model is developed to analyze the effects of BLI on the lift and drag aerodynamic characteristics.

Findings – Subsequently, detailed computational analyses are conducted at different flight states, and the regularities under various flight altitudes and velocities are revealed. Computational results demonstrate that BLI can improve the lift to drag ratio evidently and enable a great performance potentiality.

Practical implications – The general analysis method and useful regularities have reference value to DPC aircraft and other similar aircrafts.

Originality/value – This paper proposed a DPS model-based comprehensive analysis method of BLI benefit on aerodynamics for DPC aircraft, and the unique aerodynamics of this new configuration under various flight altitudes and velocities was revealed.

Keywords Computational fluid dynamics, Aerodynamic characteristics, Boundary layer ingestion, Distributed propulsion configuration

Paper type Research paper

Nomenclature

Symbols

A_1 = cross section of inlet, m^2;
A_8 = nozzle exit area, m^2;
C_L = lift coefficient, dimensionless;
C_D = drag coefficient, dimensionless;
E_{re} = power consumption, W;
F = thrust, N;
f = fuel to air ratio, dimensionless;
H_e = enthalpy function, J;
h = flight altitude, m;
K = flow coefficient, dimensionless;
M = Mach number, dimensionless;
P = static pressure, Pa;
P^* = total pressure, Pa;
q_m = air mass flow rate, kg/s;
q_{mf} = fuel flow, kg/s;
$q(\lambda)$ = flow function, kg/s;
R = gas constant, J/(kg·K);
T = static temperature, K;
T^* = total temperature, K;
V = velocity, m/s;
α = angle of attack, deg;
β_{cr} = critical pressure ratio of nozzle, dimensionless;
π = pressure ratio, dimensionless;
γ = specific heat ratio, dimensionless;
λ = velocity coefficient, dimensionless;
σ = total pressure recovery coefficient, dimensionless;
η = efficiency coefficient, dimensionless; and
η_{BLI} = BLI intensity, dimensionless.

The current issue and full text archive of this journal is available on Emerald Insight at: **www.emeraldinsight.com/1748-8842.htm**

Aircraft Engineering and Aerospace Technology
91/10 (2019) 1285–1294
 [ISSN 1748-8842]
[DOI 10.1108/AEAT-06-2018-0174]

This work was supported by the National Natural Science Foundation of China (Grant No.61304030). The authors acknowledge the research object derived from the Silent Aircraft Initiative program.

Received 28 June 2018
Revised 15 April 2019
Accepted 7 May 2019

Aircraft Engineering and Aerospace Technology
Volume 91 · Number 10 · 2019 · 1285–1294

Acronym, abbreviation

BLI = boundary layer ingestion;
BWB = blended wing body;
CFD = computational fluid dynamics;
DPS = distributed propulsion system; and
DPC = distributed propulsion configuration.

Introduction

Distributed propulsion configuration (DPC) is a novel design for civil aircraft that effectively improves fuel economy and reduces pollution emission. Different from the traditional transport aircraft with thrust-generating engines either under the wings or on the fuselage to minimize aerodynamic interactions on the vehicle operation, the concept of DPC is to fully integrate a propulsion system within the airframe with the feature of distributing thrust using many propulsors such that the aircraft takes full synergistic benefits of coupling of airframe aerodynamics and the propulsion thrust (Kim, 2010). DPC is considered by some to be the future trend for commercial aviation (Dangelo, 2010; Hileman *et al.*, 2007). Compared to the conventional large civil aircraft (Liebeck, 2004), one of the probable innovations for DPC is the integration of blended wing body (BWB) layout and the semi-embedded distributed propulsion system (DPS). Engines can ingest the boundary layer on the upper surface of the fuselage, and then certainly affect the flow fields on the airframe surface, featuring the unique boundary layer ingestion (BLI) effect. The purpose of BLI is to maximize the advantage of the coupling effect between the aerodynamics and propulsion system of the DPC aircraft. With this specific BLI effect, the lift and drag aerodynamic characteristics of the DPC aircraft are significantly improved by ingesting the boundary layer flow into the engines, and the aerodynamics and propulsion system of aircraft are closely coupled. As the most important characteristic of DPC, the aero-propulsive coupling effect should be thoroughly explored to achieve the integrated flight/propulsion control of the DPC aircraft. In view of this, it is therefore necessary to systematically study the unique lift and drag aerodynamic characteristics influenced by BLI. Current research on the BLI effect includes three main aspects: assessments of the BLI effect on the engine's performance (Smith, 1993; Felder *et al.*, 2011; Plas, 2006; Kok *et al.*, 2010), inlet and nacelle design for the BLI effect (Rodriguez, 2002; Lee and Liou, 2010; Carter *et al.*, 2006) and active flow control in the inlet to decrease the adverse impact of BLI (Gorton *et al.*, 2004; Owens *et al.*, 2006; Johnson *et al.*, 2010; Harrison *et al.*, 2013). By performing a quantitative experiment on the Cambridge-MIT "Silent Aircraft," Plas found that BLI can reduce fuel burn up to 3.8 per cent (Plas, 2006). Kok *et al.*, 2010 found that the DPC configuration with three BLI engines approximately had a 5 per cent performance improvement in terms of fuel consumption over a strut mounted propulsion system (Kok *et al.*, 2010). For the inlet and nacelle design, Rodriguez *et al.* presented a design method that approached the integration problem of a semi-embedded inlet and fuselage with multidisciplinary optimization (Rodriguez, 2002). Lee *et al.* investigated the discrete adjoint method to achieve shape optimization of the surface geometry at the inlet entrance to improve the quality of incoming flow into the engine. By using the optimization procedure, the new inlet could yield the significant improvements of more than 50 per cent reduction in flow distortion and 3 per cent increase in total pressure recovery (Lee and Liou, 2010). For flow control on the BLI inlet, Owens *et al.* presented a small-scale demonstration of an active flow control system for a BLI inlet, and the data showed that the flow control jets and the vortex generators can significantly reduce circumferential distortion (Owens *et al.*, 2006). These studies focused mostly on the internal characteristics of engines, with little concern for the aero-propulsive cross coupling effects.

In 2012, Lugo *et al.*,2012 investigated the effects of BLI on the aerodynamics of a transonic wing using a two-dimensional computational model of a transonic airfoil with BLI propulsion system (Lugo *et al.*, 2012). However, the detailed DPS model was not built in the computational procedure, and consequently the detailed inlet and outlet boundary conditions for computational fluid dynamics (CFD) solution cannot be provided accurately. For the engine fan inlet, only the static pressure was assumed as the boundary condition, which was varied to change the mass flow entering the engine. Kang *et al.* also conducted a preliminary two-dimensional (2D) study on the aerodynamic characteristics with different BLI effects (Kang *et al.*, 2014). Based on a simplified 2 D sectional model of the DPC aircraft, numerical analysis of BLI influences on the lift and drag aerodynamics was carried out. Borer Nicholas *et al.* discussed the development of two design-order approaches to capture the aerodynamic-propulsive benefits of different types of distributed electric propulsion for NASA's X-57 flight demonstrator (Borer *et al.*, 2017). X-57 used multi-propulsor distributed across the leading edge of the wing, which was different from the aircraft configuration that produced the BLI effect to some extent, and the BLI coupling effect was not studied here. Kerho Michael and Wick *et al.* conducted the computational investigation into the aero-propulsive coupling effects on the distributed propulsion system. A computational model of a five-fan turbo electric-distributed propulsion geometry was developed. Subsequently the effects of different fan thrust angles and thrust levels on the sectional lift, moment were investigated (Kerho, 2015). Perry *et al.*, 2018, further carried out wind tunnel experiments on a NACA 64_3-618 airfoil model with an array of five ducted fans integrated across the upper-surface trailing edge (Perry *et al.*, 2018). On other aspects, three candidate DP configurations, namely, the upper trailing edge, the lower trailing edge and the imbedded concepts, were selected and integrated with a representative conventional aircraft to perform a baseline assessment of their aerodynamic performance in 3 D (Wick *et al.*, 2015). To model BLI effects, modified CFD boundary conditions were developed that enabled the simulation of fans running at constant power settings. The inflow boundary conditions included the calculated total temperature and total pressure. With a specified increment in the total temperature and an assumed adiabatic efficiency, downstream boundary conditions were then computed. This simplified CFD boundary condition was inadequate in accounting for BLI on the DPC aircraft.

In summary, the above established computational model and the simplified boundary conditions cannot accurately reflect the aerodynamic regularities influenced by the BLI effect.

Nonetheless, as the most important feature of the new DPC, the unique aerodynamics with the BLI effect should be investigated systematically and thoroughly.

To overcome this, a DPS model-based comprehensive analysis method is proposed to accurately investigate the BLI effect. It uses a detailed DPS mathematical model to provide the actual CFD boundary conditions and guarantee the accuracy of the BLI simulation. Then a synthetic 3-D computational model is built to analyze the aerodynamic characteristics with different BLI intensities. Moreover, model-based computational analyses are conducted at different flight states, and the useful regularities under various flight altitudes and velocities are revealed. As a general analysis method for DPC, the common calculation process and regularities in this paper have reference value to other similar aircrafts.

This paper is organized as follows. The illustration of the BLI effect is presented first. This section is then followed by the detailed modeling process of all the DPS components. Then, the description of the comprehensive analysis method is described in detail, after which, BLI influences on the aerodynamic characteristics at different flight states are investigated by the CFD computation. Finally, conclusions are stated in the final section.

Illustration of the boundary layer ingestion effect

For the DPC aircraft, the distributed propulsion system is usually semi-embedded on the upper rear edge of the BWB fuselage, leading to the typical aerodynamic effect, BLI. The initiative purpose of BLI is to ingest the wake flow on the upper surface of the fuselage into distributed engines and effectively improve fuel economy. The BLI effect is illustrated in Figure 1.

The BLI intensity η_{BLI} is defined as:

$$\eta_{BLI} = \frac{A_\infty}{A_1} \tag{1}$$

where A_1 refers to the cross-section of the engine's inlet and A_∞ refers to a cross-section far ahead perpendicular to the air flow velocity with the same mass flow rate as A_1.

According to the air mass flow rate expression $q_m = KP^*A_i q(\lambda_i)/\sqrt{T^*}$, the BLI intensity [equation (1)] can be further expressed as:

$$\eta_{BLI} = \frac{q(\lambda_1)}{q(\lambda_\infty)} \tag{2}$$

Figure 1 Illustration of BLI effect

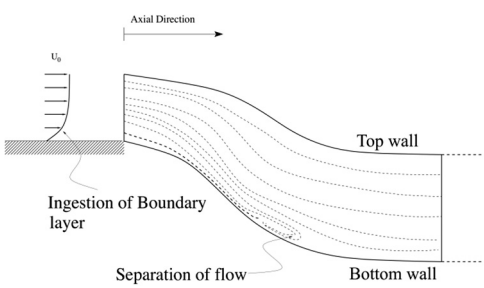

where P^* and T^* are the total pressure and the total temperature, respectively. K is the flow coefficient, and $q(\lambda_i)$ represents the flow function, which is defined as:

$$q(\lambda_i) = \left(\frac{\gamma+1}{2}\right)^{\frac{1}{\gamma-1}} \lambda_i \left(1 - \frac{\gamma-1}{\gamma+1}\lambda_i^2\right)^{\frac{1}{\gamma-1}} \tag{3}$$

where γ is the specific heat ratio and λ_i is the velocity coefficient related to Mach number. The subscript i represents the different cross sections.

Modeling process of distributed propulsion configuration

A typical DPC aircraft with three engines is selected as the research object in this paper (Hileman *et al.*, 2007). It uses a three-engine configuration with nine fans to achieve the benefits of distributed propulsion. Each engine has a single core with one low pressure turbine to drive three fans. A transmission system is used to divide and transmit the required power from the turbine into the distributed fans (Blanco *et al.*, 2007). The components of each engine include the inlet, distributed fans, the core-engine compressor, the burner, the turbine and the variable exhaust nozzle. The layout of each engine is illustrated in Figure 2.

In which, "∞" represents the region in the undisturbed airflow far ahead, "1" represents the entrance of the inlet, "2" and "3" represent the entrance and exit of distributed fans, respectively, "4" represents the exit of the core-engine compressor, "5" and "6" represent the front and rear sections of the turbine and "8" represents the exit of the exhaust nozzle. The DPS model is built on the basis of the inherent characteristics and the thermodynamic process of all components, and the detailed modeling process of each engine is described as follows.

Characteristic equations of components

As the distributed engines are embedded on the upper surface of the fuselage, the fan inlet is not freestream flow as in a conventional aircraft but partly boundary flow. As a consequence, the following assumptions are introduced in the components modeling:

- All the inlet flows are fully mixed before entering propulsors.
- No fan efficiency drops because of inlet distortion (Liu *et al.*, 2012).

Inlet

Suppose that the flight altitude and Mach number are h, M respectively, and then the static pressure, the static temperature and the freestream velocity (P_0, T_0, V_∞) of the undisturbed airflow can be determined. According to P_0, T_0, the entrance parameters of the inlet can be calculated by:

$$P_1^* = P_0\left(1 + \frac{\gamma-1}{2}M^2\right)^{\frac{\gamma}{\gamma-1}} \tag{4}$$

Figure 2 Layout of each engine

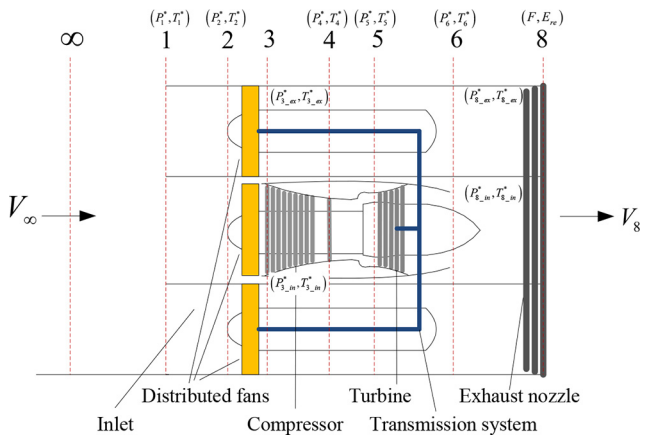

$$T_1^* = T_0\left(1 + \frac{\gamma - 1}{2}M^2\right) \tag{5}$$

where P^* and T^* are the total pressure and temperature, respectively. Numbers in the subscripts represent the corresponding stations in Figure 2.

The total pressure recovery coefficient σ_i is selected to represent the loss of total pressure in the inlet, consequently the characteristic component equations are expressed as:

$$P_2^* = \sigma_i * P_1^*,\ T_2^* = T_1^* \tag{6}$$

Distributed fans are shown in Figure 2. The distributed fans include one core-engine fan and two propulsor fans on each side. The air flow in distributed fans is approximately considered as the isentropic process. Then based on [equation (6)], the thermodynamic equations of all fans can be expressed as below:

$$P_{3\_ex}^* = \pi_{f\_ex} * P_2^* \tag{7}$$

$$P_{3\_in}^* = \pi_{f\_in} * P_2^* \tag{8}$$

$$T_{3\_ex}^* = \left(1 + \left(\pi_{f\_ex}^{\frac{\gamma-1}{\gamma}} - 1\right)\frac{1}{\eta_{f\_ex}}\right) * T_2^* \tag{9}$$

$$T_{3\_in}^* = \left(1 + \left(\pi_{f\_in}^{\frac{\gamma-1}{\gamma}} - 1\right)\frac{1}{\eta_{f\_in}}\right) * T_2^* \tag{10}$$

$$E_{ref} = \frac{2\gamma}{\gamma - 1}R\left(T_{3\_ex}^* - T_2^*\right) * q_{m\_ex} + \frac{\gamma}{\gamma - 1}R\left(T_{3\_in}^* - T_2^*\right) * q_{m\_in} \tag{11}$$

where P_3^* and T_3^* are the total pressure and temperature at the fan exit, π_f, η_f and q_m are the fan pressure ratio, the fan efficiency and the air mass flow, respectively. Subscripts *ex* and *in* refer to the propulsor fans and the core-engine fan, respectively. R is the gas constant, E_{ref} is the total required power of distributed fans.

Core-engine compressor

For the internal duct, the air flow in the core-engine compressor has the similar thermodynamic process to the distributed fans. Hence, based on [equations (8) and (10)], the parameters at the core-engine compressor exit can be calculated by:

$$P_4^* = \pi_c * P_{3\_in}^* \tag{12}$$

$$T_4^* = \left(1 + \left(\pi_c^{\frac{\gamma-1}{\gamma}} - 1\right)\frac{1}{\eta_c}\right) * T_{3\_in}^* \tag{13}$$

$$E_{rec} = \frac{\gamma}{\gamma - 1}R\left(T_4^* - T_{3\_in}^*\right) * q_{m\_in} \tag{14}$$

where π_c and η_c are the compressor pressure ratio and efficiency, respectively. E_{rec} refers to the required power of the core-engine compressor.

Burner

After the core-engine compressor, the high-pressure air enters into the burner to fully mix with fuel flow. Two important parameters of the burner are the total pressure recovery coefficient σ_b and the burn efficiency η_b.

Assume the fuel flow is q_{mf}, thus the burner exit mass flow is $q_{m5} = q_{mf} + q_{m\_in}$ with the corresponding fuel to air ratio is:

$$f = q_{mf}/q_{m\_in} \tag{15}$$

According to the enthalpy function $H_e = (T^*, f)$, the enthalpy value of the burner entrance H_4 can be determined as $H_4 = g(T_4^*, f)$. Then the burner exit enthalpy value H_5 is calculated as below:

$$H_5 = \frac{q_{m\_in} * H_4 + q_{mf} * H_u\eta_b}{q_{m5}} \tag{16}$$

where H_u is the fuel heat value. Correspondingly the burner exit temperature T_5^* is obtained.

Based on the characteristic parameter σ_b, the total pressure at the burner exit is also calculated as:

$$P_5^* = \sigma_b * P_4^* \tag{17}$$

Turbine

The purpose of the turbine is to transmit the required power to distributed fans. On the basis of the turbine entrance pressure and temperature P_5^*, T_5^*, the turbine exit parameters can be determined as:

$$P_6^* = \frac{P_5^*}{\pi_g} \tag{18}$$

$$T_6^* = T_5^*\left[1 - \left(1 - \frac{1}{\pi_g^{\frac{\gamma-1}{\gamma}}}\right)\eta_g\right] \tag{19}$$

where π_g and η_g are the turbine pressure ratio and efficiency, respectively.

The power provided to distributed fans is calculated by:

$$E_{gT} = q_{m5}\left(g\left(T_5^*, f\right) - g\left(T_6^*, f\right)\right) \tag{20}$$

Nozzle

The air flow in the nozzles can be approximately regarded as the isentropic process. Then for the internal and external nozzles, according to [equations (7) and (9)], the total pressure and temperature at the exit are obtained as below:

$$T_{8\_in}^* = T_6^*,\ T_{8\_ex}^* = T_{3\_ex}^* \tag{21}$$

$$P_{8\_in}^* = \sigma_n * P_6^*,\ P_{8\_ex}^* = \sigma_n * P_{3\_ex}^* \tag{22}$$

where σ_n represents the pressure loss in the nozzle. ($P_{8\_in}^*$, $T_{8\_in}^*$) and ($P_{8\_ex}^*$, $T_{8\_ex}^*$) are the characteristic parameters of the internal and external nozzles, respectively.

Supplementary equations

The propulsive power generated by the turbine is the sum of the actual power to the propulsor fans and the required power in the core-engine. The equation is expressed as:

$$E_{gT} = E_{ref} + E_{rec} \tag{23}$$

Furthermore, the compressed air at the nozzle exit should be checked whether it fully expands, and the corresponding expressions satisfy:

$$\begin{cases} P_{8\_in} = \dfrac{P_6^*}{\beta_{cr}} & \dfrac{P_6^*}{P_0} > \beta_{cr} \\ P_{8\_in} = P_0 & \dfrac{P_6^*}{P_0} < \beta_{cr} \end{cases} \tag{24}$$

$$\begin{cases} P_{8\_ex} = \dfrac{P_{3\_ex}^*}{\beta_{cr}} & \dfrac{P_{3\_ex}^*}{P_0} > \beta_{cr} \\ P_{8\_ex} = P_0 & \dfrac{P_{3\_ex}^*}{P_0} < \beta_{cr} \end{cases} \tag{25}$$

where P_{8_in} and P_{8_ex} refer to the static pressure of the internal nozzle and the external nozzle, respectively, β_{cr} is the critical pressure ratio of nozzle, and $\beta_{cr} = \left(\frac{2}{\gamma+1}\right)^{\frac{\gamma-1}{\gamma}}$.

Thrust and power consumption

On the basis of the above characteristic [equations (21) and (22)] and supplementary conditions [equations (24) and (25)], the intrinsic net thrust F and the power consumption E_{re} of each engine can be obtained:

$$\begin{cases} F = q_{m5}(V_{8\_in} - V_1) + (P_{8\_in} - P_0)A_{8\_in} + 2[q_{m\_ex}(V_{8\_ex} - V_1) + (P_{8\_ex} - P_0)A_{8\_ex}] \\ E_{re} = \dfrac{2\gamma}{\gamma-1}R\left(T_{3\_ex}^* - T_2^*\right) * q_{m\_ex} + \dfrac{\gamma}{\gamma-1}R\left(T_4^* - T_2^*\right) * q_{m\_in} \end{cases} \tag{26}$$

where V_1 and V_8 represent the inlet velocity and the nozzle exit velocity, respectively. A_8 is the nozzle exit area. Subscripts *in* and *ex* refer to the internal and external nozzles, respectively.

By synthesizing the three-engine characteristic equations, a complete DPS model can be obtained. This model describes the relationships among flight states (h, M), control parameters (π_f, A_8), and output variables of the propulsion system, i.e. the sectional parameters (T^*, P^*), net thrust and power consumption (F, E_{re}) and the BLI intensity η_{BLI}.

Description of the distributed propulsion configuration model-based analysis method

To accurately investigate the BLI effect, a new comprehensive analysis method based on the DPS mathematical model and CFD is proposed in this section. The DPS model designates sectional feature parameters at the engine inlet and outlet as the actual boundary conditions in CFD computation. A synthetic 3-D CFD model is designed to fully use the provided boundary conditions to simulate the boundary layer ingesting process. In view of the comprehensive composition of the DPS model and CFD computation, the BLI effect at different flight states can be calculated reliably, thereby providing conclusive data in support of the change regularities.

The overall scheme of the comprehensive analysis method is shown in Figure 3.

As shown, the scheme has three major parts:

1. First is the overall shape model including the blended-wing-body airframe and the embedded distributed propulsion system. Each distributed engine has separate control parameters to represent different intensities of BLI.
2. The second is the DPS mathematical model, which is developed on the basis of the inherent characteristics of engine components. The DPS model provides the actual feature parameters at the engine inlet and nozzle exhaust outlet. Different feature parameters correspond to different BLI effects.
3. DPS model-based CFD calculations proceed subsequently.

Based on the shape construction and the DPS mathematical model, a synthetic 3-D computational model is built in the CFD environment, which is illustrated in Figure 4.

By changing the engine's inlet and outlet feature parameters, different BLI effects are represented and the aircraft aerodynamic characteristics, including lift and drag coefficients, can be numerically calculated by CFD correspondingly. The inlet and outlet boundary conditions of DPS are set as the flow entrance and the velocity exit. The boundary conditions contain engine's inflow parameters including the static temperature T_1, the static pressure P_1 and the air flow rate q_m, as well as engine's outflow parameters

Figure 3 Scheme of the comprehensive analysis method

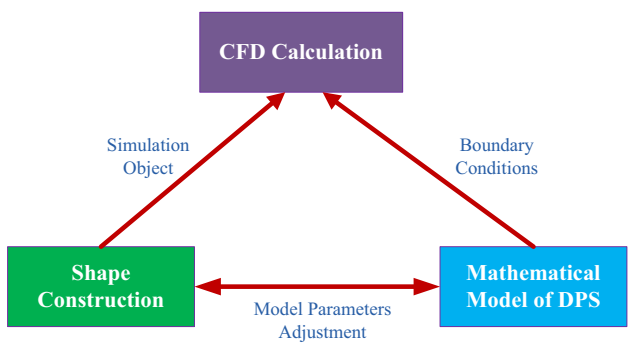

including the static temperature T_8, the static pressure P_8 and the jet velocity V_8. These boundary parameters can be calculated by the DPS mathematic model described above.

During CFD computations, there are six main procedures:

1 Current flight states including the altitude h and Mach number M are determined.
2 Aerodynamic reference values are obtained by CFD with a 3-D computational model without engines.
3 Based on the reference values of aerodynamic parameters, flight/propulsion matching analysis with the DPS model is conducted to determine the range of thrust, as well as to determine the range of DPS's control parameters and the corresponding BLI intensity.
4 According to the DPS's control parameters, the corresponding boundary conditions are extracted from the outputs of the DPS model.
5 The representative compute nodes are further extracted from the boundary conditions.
6 CFD computations are conducted on each selected node, and then the BLI effect can be explored.

Boundary layer ingestion benefits on aerodynamics at different flight states

BLI benefits on aerodynamics under different flight states are investigated systematically in this section. For the conceptual DPC commercial airliner, the cruise Mach range is approximately from Mach number 0.6 to 0.8. References indicate that the cruise speed of the latest generation SAX-40 is designed as Ma = 0.8, and the conceptual baseline airliner B-20 is designed to cruise at Mach 0.6 (Dangelo, 2010; Hileman *et al.*, 2007). Besides, the CFD computations for the typical conceptual DPC aircraft are conducted for flight Mach numbers ranging from 0.5 to 0.85 (Hileman *et al.*, 2007; Hileman *et al.*, 2010). In addition, the usual cruising altitude range is mainly about 8,000-12,000 m for most civil airliners. On the base of the above analysis, two typical flight states $h = 10{,}000$ m, $M = 0.6$ and $h = 10{,}000$ m, $M = 0.8$ are first selected to conduct the preliminary benefit analysis on the BLI effect. The descriptions of type of solver, mesh density and turbulence model that we used to carry out CFD calculations are presented in Table I.

Figure 5 shows the velocity and pressure plots of the DPC aircraft with different BLI intensities $\eta_{BLI} = 0.97, \eta_{BLI} = 1.18$, at $h = 10{,}000$ m, $M = 0.6$. The lift and drag coefficients C_L, C_D with different BLI intensities $\eta_{BLI} \in [0.9,1.2]$ are calculated and shown in Figure 6.

Figure 4 3 D computational model

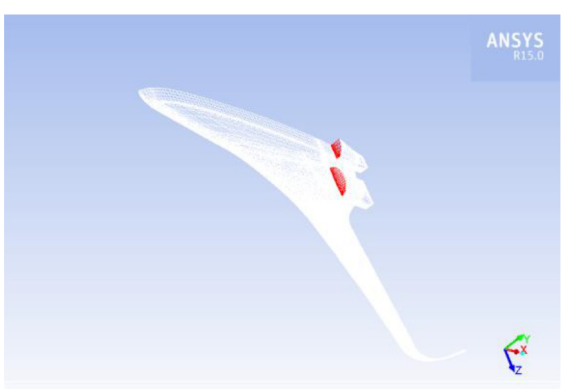

As can be seen in Figure 5, BLI has a significant effect on the velocity and pressure characteristics of the DPC aircraft. Compared to the plots of $\eta_{BLI} = 0.97$ to $\eta_{BLI} = 1.08$, it can be easily found that the boundary flow in front of the engine inlet is sucked into the engine, and the flow velocity on the upper surface of airfoil is obviously raised with the larger BLI intensity. As a result, the static pressure on the upper surface decreases apparently, especially an ultra-low pressure area is appeared near the engine inlet.

Figure 6 shows that BLI can significantly affect the aerodynamic characteristics. Although the BLI intensity is increasing, the lift coefficient C_L increases simultaneously, which is coordinated with the CFD computation results shown in Figure 5. Comparisons between different angle of attack $\alpha = 0^{\circ}$ and $\alpha = 2^{\circ}$ reveal that the lift coefficient with $\alpha = 0^{\circ}$ generally has a larger augment due to the BLI influence. On the contrary, the drag coefficient C_D decreases just to a relatively small extent with the increasing BLI intensity, and the maximum variation range inducing by BLI is up to 2 per cent approximately. The influence of BLI on the drag coefficient is mainly reflected in the pressure drag. As engines can ingest the boundary layer on the upper surface of the fuselage, the static pressure in front of the engine inlet decreases apparently and then the pressure drag of the propulsion system also reduces. However, the effect of BLI may also cause different pressure layers on the airframe surface, and this phenomenon is more prominent with the increasing BLI intensity and angle of attack. The different pressure layers may cause the additional pressure drag. Therefore, the change of the drag coefficient reflects the comprehensive influence of the above two factors. In summary, these curves indicate that the BLI effect can effectively raise the aerodynamic lift coefficient and improve the lift to drag ratio of the DPC aircraft.

Figure 7 (a)-(d) shows the velocity and pressure plots of different BLI intensities at $h = 10{,}000$ m, $M = 0.8$, and the corresponding lift and drag coefficients C_L, C_D are shown in Figure 7 (e) and (f).

As shown in Figure 7, the velocity and pressure distribution of the DPC aircraft at the higher velocity $M = 0.8$ are also significantly affected by BLI. Compared to the plots shown in Figure 5, the air flow on the upper surface especially in front of the engine inlet observably accelerates, and then the corresponding static pressure decreases consequently. Moreover, a low-speed turbulence region occurs near the nacelle, whereas the BLI intensity is weak, meaning that the flow field on the upper surface of the fuselage can be partly contaminated by this turbulence region and thus the friction drag may be increased.

Comparisons of the curves in Figure 7(e) indicate that its variation range ΔC_L inducing by the BLI effect is generally

Table I Description of solver, mesh density and turbulence model

Items	Description
Type of solver	Density-based implicit solver
Turbulence model	Spalart–Allmaras
Mesh density	
Reference length (RL)	25% MAC
Number of cells	5×10^6
Minimum mesh size	$10^{-5} \times$RL

Figure 5 Velocity and pressure plots of $h = 10{,}000$ m, $M = 0.6$

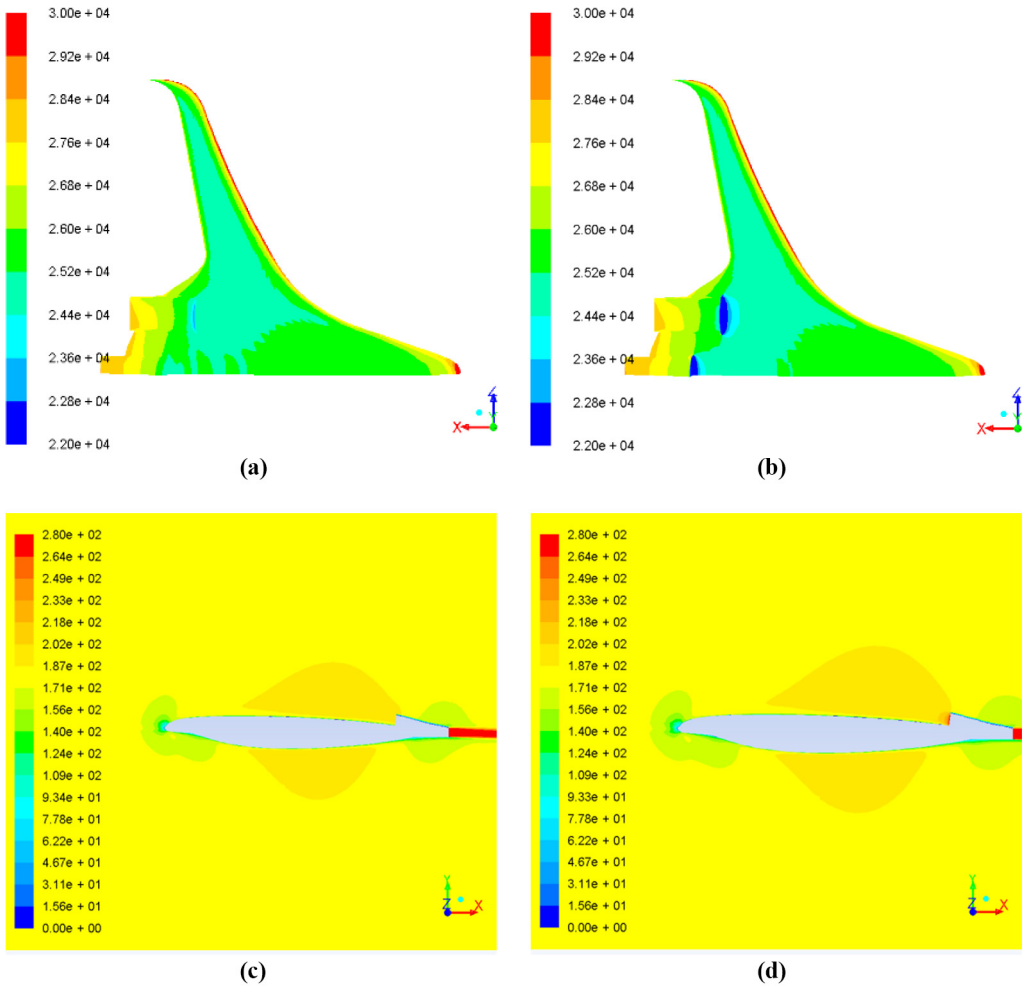

Notes: (a) Pressure plot, pascal, $\eta_{BLI} = 0.97$; (b) pressure plot, pascal, $\eta_{BLI} = 1.18$; (c) velocity plot, m/s, $\eta_{BLI} = 0.97$; (d) velocity plot, m/s, $\eta_{BLI} = 1.18$

Figure 6 Aerodynamic coefficients at $h = 10{,}000$ m, $M = 0.6$

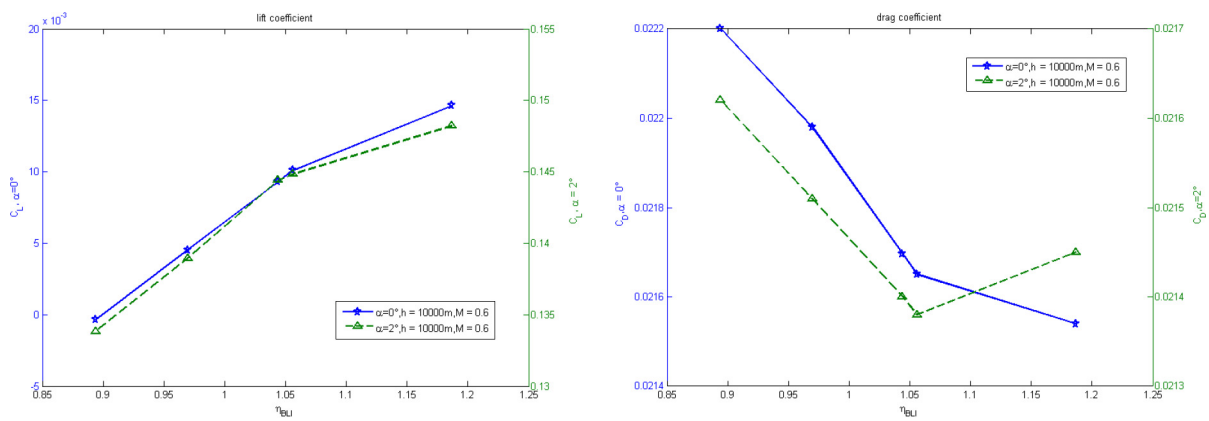

Notes: (a) Lift coefficient; (b) drag coefficient

Figure 7 Aerodynamic coefficients at $h = 10{,}000$ m, $M = 0.8$

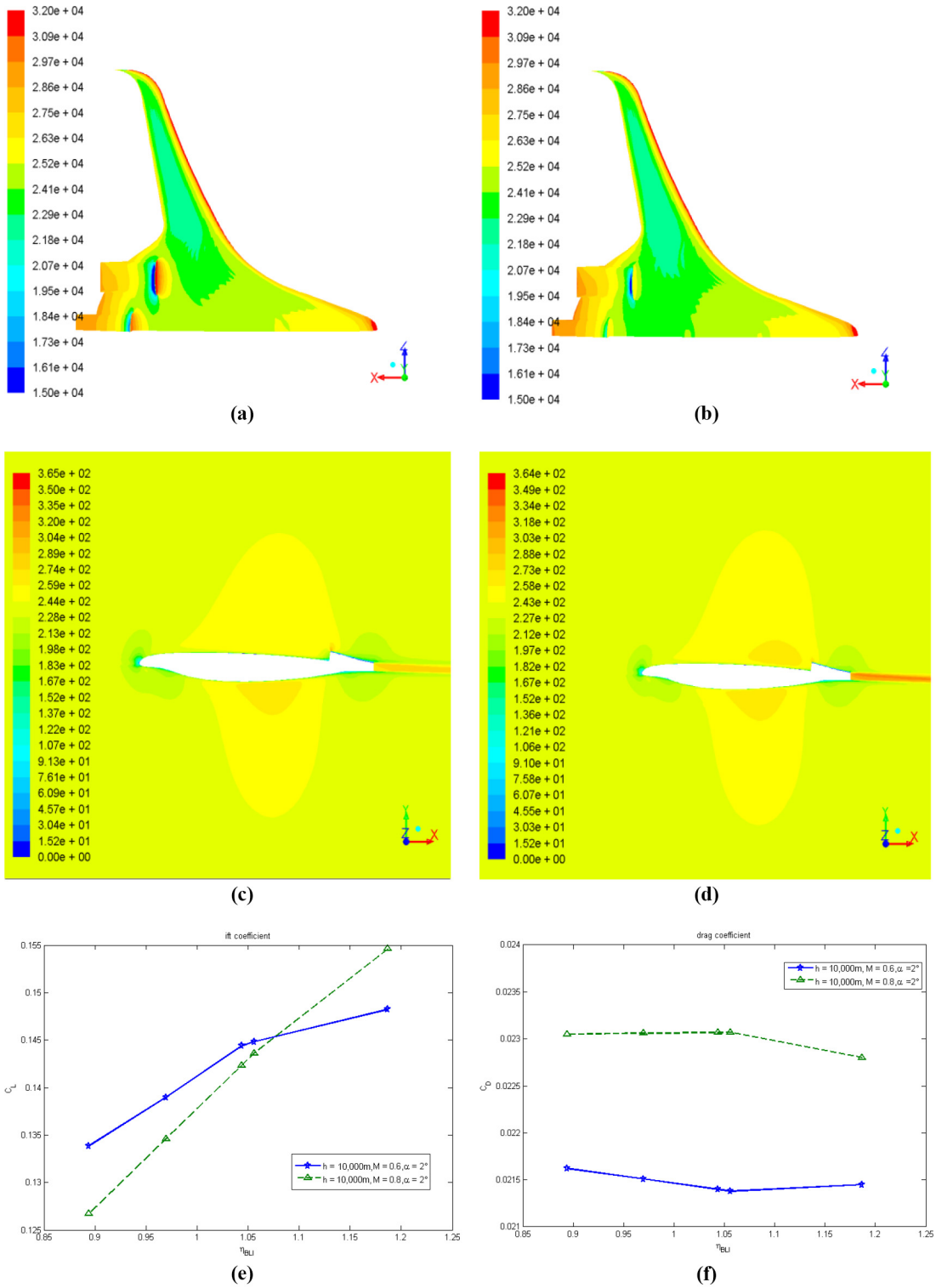

Notes: (a) Presssure plot, pascal, $\eta_{BLI} = 0.97$; (b) pressure plot, pascal, $\eta_{BLI} = 1.18$; (c) velocity plot, m/s, $\eta_{BLI} = 0.97$; (d) velocity plot, m/s, $\eta_{BLI} = 1.18$; (e) lift coefficient; (f) drag coefficient

Figure 8 Aerodynamic coefficients under different flight altitudes

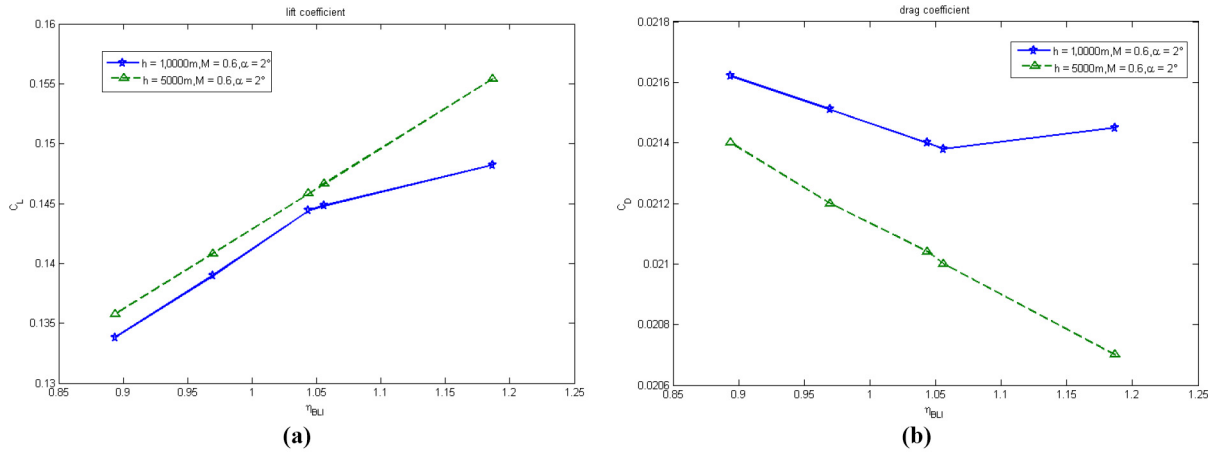

(a) (b)

Notes: (a) Lift coefficient; (b) drag coefficient

larger at the higher speed, meaning that the improvement of the aerodynamic lift by BLI tends to be relatively enhanced. For the drag coefficient, its value just varies in a small range with the increasing BLI intensity shown in Figure 7 (f). The curves reveal that the drag-reducing ability of BLI is not as obvious as the lift. Generally, the ability of BLI to improve the lift to drag ratio would be enhanced when the flight velocity increases.

Then the flight state $h = 5{,}000\ m$, $M = 0.6$ is selected to analyze BLI influences on aerodynamics under different flight altitudes. The results for different altitudes are shown in Figure 8.

Comparing the two aerodynamic coefficients illustrations in Figure 8, the common feature of the lift coefficient C_L is that it will increase monotonously along with the intensifying BLI effect, whereas the drag coefficient C_D decreases simultaneously. However, the differences are also obvious. First, the aerodynamic parameters at $h = 5{,}000\ m$ vary linearly throughout the entire BLI intensity range $\eta_{BLI} \in [0.9, 1.2]$. Moreover, their variation ranges $\triangle C_L, \triangle C_D$ related to BLI are apparently larger at the lower altitude, which indicates that the BLI effect would be strengthened at the lower altitude.

In conclusion, all the results demonstrate that the BLI effect can definitely improve the aerodynamic lift and the lift to drag ratio of the DPC aircraft at various flight states, including different velocities and altitudes. The change regularities illustrate that the influences of BLI on the aerodynamic lift and drag coefficients appear to be enhanced along with the increasing of velocity and decreasing of altitude. By effectively using this unique aero-propulsive coupling effect, the overall performance of the DPC aircraft can be improved remarkably.

Conclusion

BLI effect is an important feature of the aircraft with DPC. Aiming at this point, this article conducts a systematic research on the aerodynamic characteristics of the DPC aircraft with BLI effect. The propulsion-model based comprehensive analysis method is proposed, which uses the detailed mathematical model of distributed propulsion system to generate the boundary conditions. Then a synthetic 3-D computational model is built to investigate the influences of BLI on the aerodynamic characteristics at different flight states. Computational results demonstrate that BLI can improve the lift to drag ratio evidently and enable a great performance potentiality.

Further work

A point to be taken into further consideration is the benefit analysis on the BLI effect under large angle of attack and other flight phase, and it is essential to realize integrated flight/propulsion control of the DPC aircraft.

References

Blanco, E.R., Hall, C.A. and Crichton, D. (2007), "Challenges in the silent aircraft engine design", *Proceeding, 45th AIAA aerospace sciences meeting and exhibit, special session: towards a silent aircraft, 2007, Reno, NV*, pp. 1-20.

Borer, N.K., Derlaga, J.M., Deere, K.A., Carter, M.B., Viken, S. A., Patterson, M.D. and Litherland, B.L. (2017), "Comparison of aero-propulsive performance predictions for distributed propulsion configurations", *Proceeding, 55th AIAA aerospace sciences meeting, 2017, Grapevine, TX*, pp. 1-16.

Carter, M.B., Campbell, R.L., Pendergraft, O.C., Friedman, D.M. and Serrano, L. (2006), "Designing and testing a blended wing body with boundary-layer ingestion nacelles", *Journal of Aircraft*, Vol. 43 No. 5, pp. 1479-1489.

Dangelo, M.M. (2010), *N+3 Small Commercial Efficient and Quiet Transportation for Year 2030-2035*, NASA/CR-2010-216691, US, pp.1-72.

Felder, J.L., Kim, H.D., Brown, G.V. and Chu, J. (2011), "An examination of the effect of boundary layer ingestion on turboelectric distributed propulsion systems", *Proceeding, 49th AIAA aerospace sciences meeting including the new horizons forum and aerospace exposition, 2011, Orlando, FL*, pp.1-26.

Gorton, S.A., Owens, L.R., Jenkins, L.N., Allan, B.G. and Schuster, E.P. (2004), "Active flow control on a boundary-layer-ingesting inlet", *Proceeding, 42nd AIAA aerospace sciences meeting and exhibit, 2004, Reno, NV*, pp.1-12.

Harrison, N.A., Anderson, J., Fleming, J.L. and Ng, W.F. (2013), "Active flow control of a boundary layer ingesting serpentine inlet diffuser", *Journal of Aircraft*, Vol. 50 No. 1, pp. 262-271.

Hileman, J.I., Spakovszky, Z.S., Drela, M., Sargeant, M.A. and Jones, A. (2010), "Airframe design for silent fuel-efficient aircraft", *Journal of Aircraft*, Vol. 47 No. 3, pp. 956-969.

Hileman, J.I., Spakovszky, Z.S. and Drela, M. (2007), "Airframe design for silent aircraft", *Proceeding, 45th AIAA aerospace sciences meeting and exhibit*, 2007, *Reno, NV*, pp. 1-15.

Johnson, B.C., Webster, R.S. and Sreenivas, K. (2010), "A numerical investigation of S-duct flows with boundary-layer ingestion", *Proceeding, 48th AIAA aerospace sciences meeting including the new horizons forum and aerospace exposition*, 2010, *Orlando, FL*, pp.1-12.

Kang, W.W., Zhang, J. and Yang, L.Y. (2014), "Research on boundary layer ingestion effects of distributed propulsion configuration", *Proceeding, 2014 IEEE Chinese guidance, navigation & control conference*, 2014, *Yantai, China*, pp.1-8.

Kerho, M. (2015), "Aero-propulsive coupling of an embedded, distributed propulsion system", *Proceeding, 33rd AIAA applied aerodynamics conference, 2015, Dallas, TX*, pp.1-20.

Kim, H.D. (2010), "Distributed propulsion vehicles", *Proceeding, 27th International Congress of the Aeronautical Sciences, 2010, Nice, France*, pp.1-11.

Kok, H.J., Voskuijl, M. and Tooren, M.J. (2010), "Distributed propulsion featuring boundary layer ingestion engines for the blended wing body subsonic transport", *Proceeding, 51st AIAA/ASME/ASCE/AHS/ASC structures, structural dynamics and materials conference, 2010, Orlando, FL*, pp.1-12.

Lee, B.J. and Liou, M.S. (2010), "Optimizing a boundary-layer-ingestion offset inlet by discrete adjoint approach", *AIAA Journal*, Vol. 48 No. 9, pp. 2008-2016.

Liebeck, R.H. (2004), "Design of the blended wing body subsonic transport", *Journal of Aircraft*, Vol. 41 No. 1, pp. 10-25.

Liu, C.Y., Georgios, D., Panagiotis, L. and Singh, R. (2012), "Turboelectric distributed propulsion system modelling for hybrid-wing-body aircraft", *Proceeding, 48th AIAA/ASME/SAE/ASEE joint propulsion conference & exhibit, 2012, Atlanta, GA*, pp.1-13.

Lugo, V.M., Doulgeris, G. and Singh, R. (2012), "Computational analysis of the effects of a boundary layer ingesting propulsion system in transonic flow", *Proceeding IMechE Part G: Journal of Aerospace Engineering*, Vol. 227 No. 8, pp. 1215-1232.

Owens, L.R., Allan, B.G. and Gorton, S.A. (2006), "Boundary-layer-ingesting inlet flow control", *Proceeding, 44th AIAA aerospace sciences meeting and exhibit, 2006*, Reno, NV, pp.1-23.

Perry, A.T., Ansell, P.J. and Kerho, M.F. (2018), "Aero-propulsive and propulsor cross-coupling effects on a distributed propulsion system", *Journal of Aircraft*, Vol. 55 No. 6, pp. 2414-2426.

Plas, A. (2006), "Performance of a boundary layer ingesting propulsion system", Master thesis, Massachusetts institute of technology, US.

Rodriguez, D.L. (2002), "A multidisciplinary optimization method for designing boundary layer ingesting inlets", *AIAA-2002-5665, US*.

Smith, L.H. (1993), "Wake ingestion propulsion benefit", *Journal of Propulsion and Power*, Vol. 9 No. 1, pp. 74-82.

Wick, A.T., Hooker, J.R. and Hardin, C.J. (2015), "Integrated aerodynamic benefits of distributed propulsion", *Proceeding, 53rd AIAA aerospace sciences meeting, 2015, Kissimmee, FL*, pp. 1-36.

Further reading

Allan, B.G. and Owens, L.R. (2006), "Numerical modeling of flow control in a boundary-layer-ingesting offset inlet diffuser at transonic Mach numbers", *Proceeding, 44th AIAA aerospace sciences meeting and exhibit*, 2006, *Reno, NV*, pp.1-25.

Allan, B.G., Owens, L.R. and Lin, J.C. (2006), "Optimal design of passive flow control for a boundary- layer-ingesting offset inlet using design-of-experiments", *Proceeding, 44th AIAA aerospace sciences meeting and exhibit*, 2006, *Reno, NV*, pp.1-14.

Anabtawi, A.J., Blackwelder, R.F., Lissaman, B.S. and Liebeck, R. (1999), "An experimental study of vortex generators in boundary layer ingesting diffusers with a centerline offset", *Proceeding, 35th AIAA/ASME/SAE/ASEE Joint propulsion conference and exhibit*, 1999, *Los Angeles, CA*, pp.1-12.

Anabtawi, A.J. (1999), "Experimental investigation of boundary layer ingestion into diffusing inlets", Doctor Thesis, University of southern California.

Atinault, O., Carrier, G., Grenon, R., Verbecke, C. and Viscat, P. (2013), "Numerical and experimental aerodynamic investigations of boundary layer ingestion for improving propulsion efficiency of future air transport", *Proceeding, 31st AIAA applied aerodynamics conference, 2013, San Diego, CA*, pp.1-13.

Daggett, D.L. Kawai, R. and Friedman, D. (2003), "Blended wing body systems studies: boundary layer ingestion inlets with active flow control", NASA/CR-2003-212670, US.

Elmiligui, A.A., Fredericks, W.J., Guynn, M.D. and Campbell, R.L. (2013), "Numerical investigation of a fuselage boundary layer ingestion propulsion concept", *Proceeding, Aviation technology, integration, and operations conference*, 2013, *Los Angeles, CA*, pp.1-18.

Freuler, P.N. (2005), "Boundary layer ingesting inlet design for a silent aircraft", Master thesis, Massachusetts institute of technology, US.

Parham, J.B., Fitzgerald, M., and Blanco, E.R. (2011), "Flow control for boundary layer ingestion in an s-duct diffuser", *Proceeding, 49th AIAA aerospace sciences meeting including the new horizons forum and aerospace exposition, 2011*, Orlando, FL, pp.1-9.

Corresponding author

Jing Zhang can be contacted at: zhangjing2013@buaa.edu.cn